Photodetachment Imaging Study of the Vinoxide Anion[†]

M. Shane Bowen and Robert E. Continetti*

Department of Chemistry and Biochemistry, University of California, San Diego, 9500 Gilman Drive, La Jolla, California 92093-0340

A photodetachment imaging study of the photoelectron angular distributions produced by the 354.8-nm photodetachment of the vinoxide anion, H_2C═CHO^-, is reported. The photoelectron angular distributions for both the $\tilde{X}^2A''$ ground state and $\tilde{A}^2A'$ excited state of the neutral vinoxy radicals were measured. Energy-dependent photoelectron anisotropy parameters are reported for both electronic states. Photodetachment from the HOMO of the anion (the CCO nonbonding $\pi(a'')$ orbital) yields ground-state vinoxy radicals and exhibits a $\sin^2\theta$ angular dependence ($\beta\ (\tilde{X}^2A'') = -0.7 \pm 0.1$) relative to the electric vector of the laser. Photodetachment from the HOMO-1 of the anion (the oxygen $\sigma_{2px}(a')$ orbital) yields excited-state $\tilde{A}^2A'$ radicals and exhibits a $\cos^2\theta$ angular dependence ($\beta\ (\tilde{A}^2A') = 0.6 \pm 0.1$) of the photoelectrons. These results are qualitatively interpreted in terms of the electronic structure of the anion−neutral system.

1. Introduction

The vinoxide anion and the corresponding vinoxy radical are the simplest examples of the enolate and enolate radical moieties, representing a class of organic anions and radicals important in several applications. There is considerable interest in understanding the energetics, dynamics, and electronic structure of these species[1−6] and the evolution of these properties as a function of molecular size and substitution. We have previously studied the energetics of this system[7] and larger enolates containing up to four carbons[8] using negative ion photoelectron spectroscopy. Here, we report studies of the photoelectron angular distributions for vinoxide, $C_2H_3O^-$, and the interpretation of these angular distributions in terms of the electronic structure of the anion and low-lying states of the neutral vinoxy radical.

Photoelectron spectroscopy of negative ions is a powerful way to simultaneously study the energetics and electronic structure of both the negative ion and the corresponding neutral.[9] In recent years, photodetachment imaging techniques[10−13] have complemented more traditional approaches to photoelectron spectroscopy by making facile the measurement of photoelectron angular distributions. The angular distribution of electrons photodetached from molecular negative ions provides insights into the overall symmetry of the initial anion wave function and the continuum photoelectron wave function.[12,14,15] In the studies presented here, measurement of photoelectron angular distributions from photodetachment of the C_s-symmetry vinoxide anion, H_2C═CHO^-, is exploited to investigate the symmetry of the bound and continuum molecular orbitals involved.

Photodetachment of the vinoxide anion was previously studied by Ellison and Lineberger,[16] and at higher photon energies in this laboratory by Alconcel et al.[7] The definitive value for the electron affinity of the ground-state vinoxy radical was found in a threshold photodetachment study by Mead et al. to be $1.8248 + 0.0002 - 0.0008$ eV.[17] In the work of Alconcel et al., vinoxide was detached with 354.8-nm (3.494 eV) radiation yielding stable neutral vinoxy radicals in the ground and first excited electronic states, $\tilde{X}^2A''$ and $\tilde{A}^2A'$, respectively. The electronic state separation energy between the ground and first excited states of the vinoxy radical was measured in this experiment ($T_0(\tilde{A} \leftarrow \tilde{X}) = 1.015 \pm 0.015$ eV) and was in good agreement with theoretical predictions. Although optical excitation of this state is dipole-allowed from the ground state of the radical, it involves a large change in electronic structure and geometry and thus has a very low absorption cross section, making optical studies difficult.[18,19] The vibrational structure of the $\tilde{X}$ and $\tilde{A}$ states was also investigated in these studies and analyzed using ab initio calculations and Franck−Condon simulations.[7] The focus of the present work is on the photoelectron angular distributions and therefore on the symmetry of the electronic wave function of the detached electrons from both the highest occupied molecular orbital (HOMO) and the HOMO-1 of the $\tilde{X}^1A'$ state of the vinoxide anion. In the following section, the experimental approach will be briefly discussed followed by a presentation of the measured photoelectron angular distributions and interpretation of these results in terms of the electronic structure of vinoxide and the ground and first excited states of the vinoxy radical.

2. Experimental Section

Photodetachment coincidence imaging of the vinoxide anion was carried out using a fast-ion-beam photoelectron-photofragment-coincidence spectrometer. This spectrometer allows the measurement of both photoelectron and photofragment kinetic energies and angular distributions in coincidence, thus allowing the direct discrimination of photodetachment events that lead to stable and unstable neutral species. In the experiments reported here, 354.8-nm photodetachment of vinoxide yields only stable neutral vinoxy radicals. The details of the experimental apparatus have been previously described elsewhere;[20−22] therefore, only a brief review is presented here. The photoelectron energy resolution is decreased in these imaging experiments; however, using this approach, the energy-dependent photoelectron angular distribution can be rapidly recorded.

Production of the vinoxide anion, H_2C═CHO^-, was performed using a pulsed electrical discharge ion source.[23] A 1

* Corresponding author. E-mail: rcontinetti@ucsd.edu.

kHz pulsed supersonic expansion of ethanol seeded in a 10% mixture of nitrous oxide in argon was formed by bubbling the gas mixture at 15 psig backing pressure through the ethanol at room temperature. In the pulsed-discharge ion source, vinoxide anions were formed by successive proton abstractions from ethanol by O^- formed in the dissociative attachment of electrons to N_2O.[24] The anions are cooled in the subsequent supersonic expansion, typically yielding vibrational temperatures of <300 K.[25]

The pulsed expansion was skimmed and the anions accelerated to 3 keV and re-referenced to ground potential,[26] mass-selected by time-of-flight (TOF) and transported into the laser interaction and detection chamber. The $m/e = 43$ ion packet was then perpendicularly intersected with a ∼100 ps, linearly polarized third-harmonic pulse (354.8 nm, 3.494 eV) from a mode-locked, Q-switched, cavity dumped Nd:YAG laser (Quantronix Model 116).[27] The laser was focused onto the ion packet yielding typical peak power densities of 480 MW/cm². The laser polarization was set parallel to the face of the electron detector (in the plane of the photoelectron images).

Following photodetachment, residual anions were electrostatically deflected out of the molecular beam and the resulting neutral species propagated over a 96-cm flight path to a 4-cm time- and position-sensitive microchannel-plate-based detector. If a stable molecule is produced, a single particle will strike the detector at the time and position of arrival of the parent beam. However, if dissociative photodetachment occurs, two momentum-matched fragments will be recorded. As previously noted, no dissociation of the nascent neutrals was observed within these measurements.

Photodetached electrons were extracted perpendicular to the laser and ion beams in a single-field space-focusing electron collection assembly and projected onto a 4-cm diameter time- and position-sensitive microchannel-plate-based detector.[22,28] The extraction field used to collect all photodetached electrons was ∼23 V/cm. To minimize perturbation of the incident ion beam, the extraction field was pulsed on approximately 140 ns prior to the laser−anion interaction. The explicit measurement of both the position and TOF for each photodetachment event allows the determination of the three-dimensional velocity distribution of the photoelectrons over the full 4πsr solid angle. Since the electron velocity *vector* is measured, both the center-of-mass electron kinetic energy (eKE) and laboratory frame photoelectron angular distributions are directly recorded. The *x*- and *y*-velocity components of the photoelectrons are determined directly from the *x,y* position information and TOF. The *z* velocity component is also determined from the TOF of the detected electron and is the limiting factor in the energy resolution.

The overall resolution in eKE is ∼14% $\Delta E/E$, determined from calibration with O^-. However, selecting photoelectrons with minimal *z*-velocity components yields higher resolution (∼10% $\Delta E/E$ in O^-) sliced photoelectron spectra. The intensity distribution in these sliced photoelectron spectra is significantly affected by the effective detector−acceptance function (DAF). A rapidly decreasing fraction of photoelectrons are detected in a given equatorial slice as the photoelectron velocity increases. The data in an equatorial slice can be corrected for the DAF when the laser electric (**E**) vector is in the plane of the slice, parallel to the electron detector. The cylindrical symmetry around the **E** vector then allows for the intensity in a given sliced velocity distribution to be corrected by the fraction of all events in the slice. Defining the azimuthal fraction of detected photoelectrons in a given *z*-velocity component slice $\pm v_z^{slice}$ as
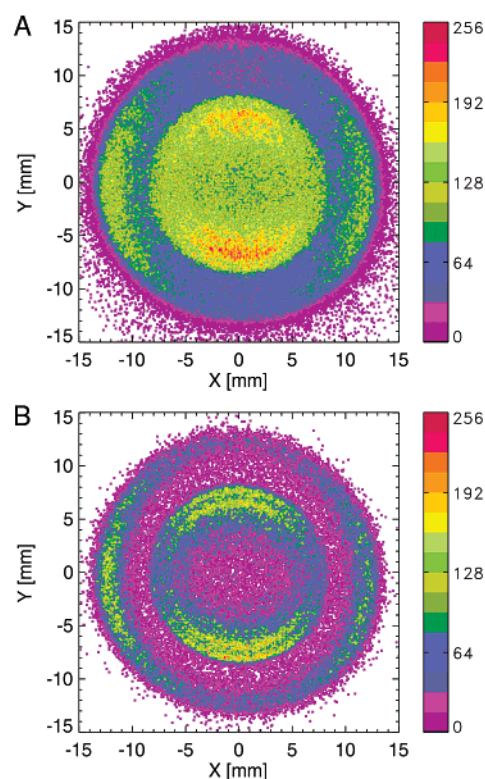

Figure 1. (a) Photoelectron image of vinoxide anions photodetached with 354.8-nm photons. The electric field vector, **E**, is parallel to the *y*-axis. All of the collected electrons summed over 10 data sets are shown. The images are presented in false color representing the total number of electrons detected at that position as shown in the legend. (b) Velocity sliced photoelectron image of vinoxide anions photodetached with 354.8-nm photons. The **E** vector is parallel to the *y*-axis. Only those collected electrons, summed over the same 10 data sets as that used in Figure 1a, with maximum $v_z = \pm0.008$ cm/ns are shown.

$\Delta\varphi_z = 2\pi/(\sin^{-1}(v/v_z^{slice}))$, the corrected intensity distribution in velocity space can be expressed as $P(v_{eKE})^{corr} = N(v_{eKE})^{slice}/2\Delta\varphi_z$, similar to the approach used in slice imaging of photofragments with CCD camera detection.[29−31] The photoelectron spectra presented here are these higher-resolution DAF-corrected sliced photoelectron spectra.

3. Results

The raw photoelectron image recorded from photodetachment of vinoxide at 354.8 nm is shown in Figure 1a. The higher-resolution velocity-sliced photoelectron image of the same data set is shown in Figure 1b. These images are a sum of 10 data sets with Figure 1a depicting all detected electrons acquired (∼575 000 events) and Figure 1b showing only detected electrons with the velocity constraint of $v_z = \pm0.008$ cm/ns (∼87 000 events). The maximum electron velocity upon photodetachment from vinoxide at 354.8 nm (3.494 eV), given the EA = 1.8 eV is 0.077 cm/ns. This velocity constraint in the data slicing restricts acceptance of events to only those electrons with a maximum of ∼10% of their velocity perpendicular to the detector.

The images exhibit two distinct structures. At large radii, corresponding to high eKE, the intensity peaks perpendicular to the laser **E** vector, while at smaller radii, corresponding to low eKE, the intensity peaks along the **E** vector. This shows that photodetachment to the ground and excited states of the vinoxy radical involve very different photodetachment transitions. The feature at large radii corresponds to those photode-

Photodetachment Imaging Study

J. Phys. Chem. A, Vol. 108, No. 39, 2004 **7829**
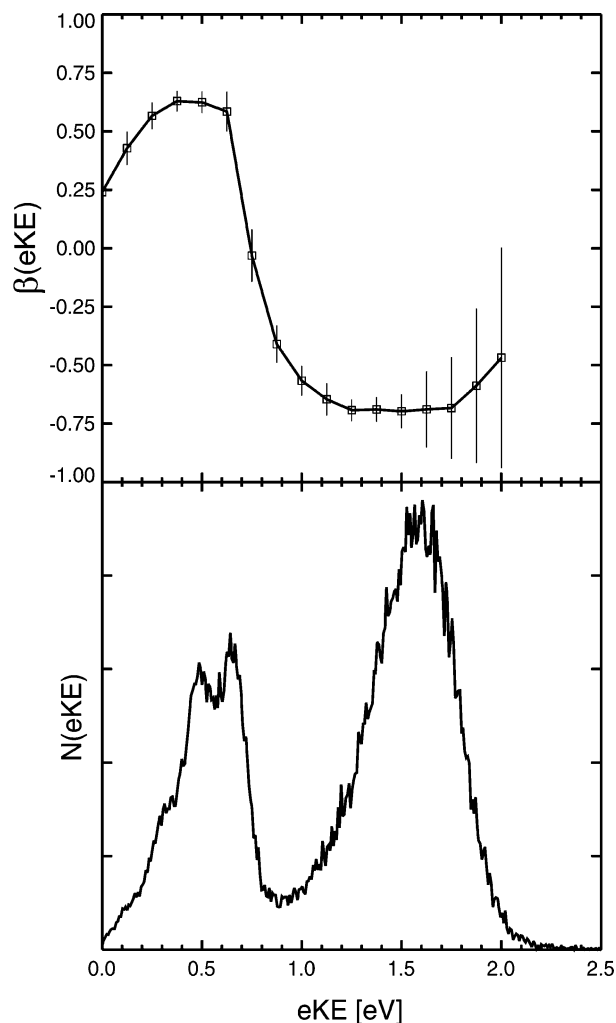
Figure 2. Anisotropy parameter β(eKE) spectrum for vinoxide photodetached at 354.8 nm. The top plot is the fit of β(eKE) in eq 1 to the experimentally measured N(eKE,θ) and the bottom plot is the DAF-corrected N(eKE) distribution. Error bars in the β(eKE) spectrum are $\pm\sigma$. Both of these spectra were produced from only those detached electrons with maximum $v_z = \pm0.008$ cm/ns.

tachment events leaving neutral vinoxy radicals in the ground electronic state. The features at small radii correspond to those photodetachment events producing the lowest electronically excited state of the neutral vinoxy radical. The enhanced resolution obtained by performing the velocity slicing is easily observed in Figure 1b by the rings corresponding to vibrational excitation in the electronically excited neutral present in the inner region of the image.

The spatial distribution of photoelectrons can be characterized in the electric-dipole approximation by the energy-dependent anisotropy parameter, β(eKE). The anisotropy parameter can be determined directly from the DAF-corrected photoelectron energy and angular distributions by fitting to the functional form for electric-dipole transitions with linearly polarized light.[32]

$$P(\text{eKE},\theta) = P(\text{eKE})[1 + \beta(\text{eKE})P_2(\cos\theta)] \qquad (1)$$

In this equation, θ is the electron recoil angle relative to the laser **E** vector (along the y-axis of the images), P(eKE) is the measured electron kinetic energy probability distribution, and $P_2(\cos\theta)$ is the second-order Legendre polynomial in $\cos\theta$. P(eKE,θ) is the normalized doubly differential cross section in eKE,θ and β(eKE) is the energy dependence of the anisotropy

parameter determined in the fit. For single-photon electric-dipole transitions, β(eKE) is restricted in value to the range from -1 to 2.

The β(eKE) spectrum from the photodetachment of the vinoxide anion at 354.8 nm is fitted to eq 1 and plotted in the upper half of Figure 2. The N(eKE) spectrum, obtained from the sliced photoelectron kinetic energy distribution, is shown in the lower half of the figure. The N(eKE) spectrum is consistent with that previously reported and clearly resolves the two electronic states being accessed. As seen in Figure 1b, some vibrational structure is observed in the region of low kinetic energy associated with excited-state photodetachment. This structure, and that present for ground-state photodetachment, was previously measured with greater resolution in the experiments of Alconcel et al.[7]

The β(eKE) spectrum in Figure 2 is consistent with the qualitative description of the images in Figures 1a and 1b given above. The inner region of the images corresponds to photodetached electrons with a high binding energy. The anisotropy parameter associated with the onset of the $\tilde{A}^2A'$ electronically excited state has a value β(eKE = 0.625 eV) = 0.6 $\pm$ 0.1. This feature results from photodetachment of the HOMO-1 orbital in the anion. A positive value for the anisotropy parameter is associated with photoelectrons scattering predominantly along the **E** vector of the laser, yielding a $\cos^2\theta$ intensity distribution. The outer region of the images corresponds to photodetached electrons with a low binding energy, correlated with the ground $\tilde{X}^2A''$ state of the vinoxy radical. The anisotropy parameter associated with this region of β(eKE) for eKE > 0.8 eV has an average value $<\beta(\tilde{X}^2A'')> = -0.7 \pm 0.1$ associated with the broad peak at high eKE resulting from photodetachment of the HOMO of the anion. A negative value for the anisotropy parameter is consistent with photodetached electrons scattering perpendicular to the **E** vector of the laser, yielding a $\sin^2\theta$ intensity distribution.

4. Discussion

The anisotropic photoelectron angular distributions measured in this study contain information about the electronic structure of the anion, the neutral, and the symmetry of the wave function of the detached free electron.[12,14,15] The wave function for the composite system of free electron plus neutral molecule must conserve angular momentum upon electric-dipole photodetachment of the anion. In the atomic case, the rigorous selection rule of $\Delta l = \pm1$ holds, and thus an atomic s-orbital yields p-wave photodetachment, with a $\cos^2\theta$ angular distribution, while an atomic p-orbital leads to s- and d-wave photodetachment. Above threshold, the s and d-waves interfere, leading to a $\sin^2\theta$ angular distribution. In a molecular system, the spherical symmetry is broken and the wave function of the free electron is represented by a partial wave expansion. The resulting partial wave superposition, with each component wave-weighted by the appropriate radial dipole matrix element, determines the symmetry of the outgoing electron wave that is measured. The analogy to atomic photodetachment and group theoretical considerations provide the basis to classify the continuum orbital of the photoelectron, particularly when a limited number of partial waves describe the photodetached electron wave function.

A rigorous theoretical treatment of photodetachment entails consideration of the dipole selection rules for photodetachment of a molecular anion and a high-level electron−molecule scattering calculation. This treatment is beyond the scope of the present work. The group theoretical formalism developed by Brauman and co-workers[14] for evaluation of photodetachment

cross sections near threshold will be applied. This formalism has previously been applied to the dissociative photodetachment of molecular anions[15] and has recently been further developed by Sanov and co-workers[12] for applications above threshold in their "s and p" model. The symmetry constraints of this model restrict the continuum states for the photodetached electron to be those for which the symmetry of the direct product of the anion electronic symmetry, the transition dipole moment μ, and the final composite state of the neutral molecule plus the continuum free electron is the totally symmetric irreducible representation. Equivalent results are obtained using a purely one-electron approximation, wherein the direct product is taken of the symmetry of the anion molecular orbital from which photodetachment occurs, the transition dipole and the continuum free electron.

Ab initio studies have shown that the electronic symmetry of the vinoxide anion ground state is A′ and the symmetry of the ground and first electronically excited states of the vinoxy radical are A″ and A′, respectively.[7] The orbitals from which photodetachment occurs are the CCO nonbonding π(a″) orbital, constituting the HOMO of the anion, and the oxygen σ_{2px}(a′) orbital, which constitutes the HOMO-1 of the anion, as discussed by Alconcel et al.[7] Both of these orbitals are doubly occupied in the closed-shell anion and thus correspond to first order to the singly occupied orbitals in the radicals generated upon photodetachment. Detachment from the HOMO yields the $\tilde{X}^2A''$ vinoxy radical, which is best represented by a ·CH$_2$CH=O structure commonly called the formylmethyl radical. Detachment from the HOMO-1 leaves the $\tilde{A}^2A'$ vinoxy radical, best represented by the H$_2$C=CHO· structure commonly known as the vinyloxy radical. The vinoxide anion has C_s symmetry and thus the transition dipole has a′ symmetry along the x and y axes in the plane of symmetry and a″ symmetry along the z axis.

Photodetachment from the HOMO of the anion involves ejection of the electron from the CCO nonbonding π(a″) molecular orbital. This orbital is only composed of p atomic orbitals and has a nodal plane in the plane of symmetry, and thus nonzero angular momentum. In the atomic limit, we can approximate the angular momentum of this orbital to be $l = 1$. Application of the $\Delta l = \pm 1$ selection rule to this approximation requires the symmetry of the detached electron to be a superposition of s and d waves. Since this experiment was carried out well above threshold, the s and d waves are expected to interfere leading to a $\sin^2 \theta$ intensity distribution peaking perpendicular to the **E** vector of the laser, as observed.

The group theoretical formalism dictates that photodetachment of vinoxide to the ground $\tilde{X}^2A''$ state of the radical is allowed if the direct product A′(anion)⊗a′($\mu_{x,y}$)⊗A″(radical)⊗Ψ_{elec} must yield the totally symmetric (A′) representation for the x and y components of the transition dipole, where Ψ_{elec} is the symmetry of the wave function for the detached electron. Similarly, if the z-component of the transition moment is involved, the direct product A′⊗a″(μ_z)⊗A″⊗Ψ_{elec} = A′ must hold. This requires the symmetry of the free electron wave to be a″ (antisymmetric) for the x and y components and a′ (symmetric) for the z component. The antisymmetric continuum wave function expected for the x and y components transform like a p$_z$-orbital. In the molecular frame, however, this p$_z$ orbital is perpendicular to the $\mu_{x,y}$ directions. Since the electric-dipole transition will be favored when the E vector of the laser is aligned with the $\mu_{x,y}$ transition moments, p$_z$ wave photodetachment is expected to peak perpendicular to the **E** vector of the laser, consistent with the $\sin^2 \theta$ angular distribution observed. The symmetric

continuum wave function expected for the μ_z component in the molecular frame transforms like s, p$_x$, or p$_y$ orbitals, and thus predicts either s- or p-wave photodetachment, where once again the p$_x$,p$_y$ continuum functions peak perpendicular to the μ_z transition moments. Thus, electric-dipole photodetachment transitions along any of the principal axes can lead to the observed $\sin^2 \theta$ angular distribution, and symmetry constraints alone cannot determine if s-wave photodetachment occurs. However, the successful threshold photodetachment experiments of Mead et al.[17] show that s-wave photodetachment does in fact occur in this system, arising from the μ_z transition moment.

Photodetachment from the HOMO-1 of vinoxide involves ejection from the σ_{2px}(a′) orbital on the oxygen atom. While this orbital is primarily a 2p$_x$ orbital on the oxygen atom, the orbital has no node in the symmetry plane of the molecule and thus is expected to carry no angular momentum in the molecular frame. Making the approximation that this σ orbital is equivalent to an atomic s orbital with $l = 0$, the photodetached electron is expected to be a p wave ($l = 1$). This is consistent with the observation that photodetachment to the $\tilde{A}^2A'$ state of the vinoxy radical yields photoelectrons preferentially scattered parallel to the E vector of the laser. Although β(eKE) is positive throughout the feature associated with excited-state detachment, it is considerably less than the maximum allowed value of $\beta = 2$. This is not surprising considering the significant approximation made in applying the atomic limit to this molecular system.

Application of the group theoretical formalism to photodetachment from vinoxide to the first excited electronic state of the radical requires A′⊗a′($\mu_{x,y}$)⊗A′⊗Ψ_{elec} = A′ for the x and y components of the dipole transition moment and A′⊗a″(μ_z)⊗A′⊗Ψ_{elec} = A′ for the z component. Thus, the allowed symmetries of the free electron wave are a′ (symmetric) for the x and y components and a″ (antisymmetric) for the z component. As discussed above, the symmetric continuum wave functions transform as s, p$_x$, and p$_y$ orbitals in C_s symmetry, while the antisymmetric continuum wave function transforms as a p$_z$ orbital. In both cases, the free electron wave has the same symmetry as the transition moment, so p-wave photodetachment in this case will always lead to a $\cos^2 \theta$ angular distribution, as observed for photodetachment to the $\tilde{A}^2A'$ excited state. Symmetry considerations alone cannot rule out s-wave photodetachment in this case, but the analogy to atomic photodetachment in the previous paragraph indicates that it is unlikely. Threshold and near-threshold photodetachment studies of the excited-state photoelectron angular distribution should be able to answer this question.

These considerations show that the observed highly anisotropic photoelectron angular distributions measured for photodetachment to the ground and first excited states of the vinoxy radical are consistent with the electronic structure calculations reported by Alconcel et al.[7] Owing to the relatively low symmetry of vinoxide, these measurements of the laboratory frame photoelectron angular distributions cannot further specify the actual photodetachment transitions. Molecular frame photoelectron angular distributions would yield considerably more information. We have shown that the molecular frame photoelectron angular distributions can be measured in the dissociative photodetachment of O$_4^-$;[15] however, in the present case no dissociation occurs, so such measurements are not viable. In anionic systems with bound excited states, Neumark and co-workers have recently shown that molecular frame photoelectron angular distributions can be deduced from dipole aligned C$_2^-$,[33] extending previous work on the photoionization of neutral molecules by Zare.[34] Vinoxide may provide an opportunity to

Photodetachment Imaging Study

J. Phys. Chem. A, Vol. 108, No. 39, 2004 **7831**

apply this approach in the future, as it is known to have a dipole-bound excited state.[35]

5. Conclusion

This study reports photoelectron angular distributions from the 354.8-nm photodetachment of vinoxide anions leaving the stable neutral vinoxy radical in both its ground $\tilde{X}^2A''$ and first excited $\tilde{A}^2A'$ electronic states. The angular distributions are analyzed in terms of the previously predicted orbital structure of the parent anion and neutral radical. The observed angular distributions for electrons photodetached from the HOMO and HOMO-1 of the anion are consistent with atomic-like and group-theoretical predictions. A more quantitative interpretation of these results will require electron−molecule scattering calculations. With the increase in measurements of photoelectron angular distributions in negative ions in recent years, there is an increasing need for such calculations and the insights they can provide into the electronic structure of anions and transient species such as the vinoxy radical.

References and Notes

(1) Su, H.; Bersohn, R. *J. Chem. Phys.* **2001**, *115*, 217.
(2) Utkin, Y. G.; Han, J.; Sun, F.; Chen, H.; Scott, G.; Curl, R. F. *J. Chem. Phys.* **2003**, *118*, 10470.
(3) Matsika, S.; Yarkony, D. R. *J. Chem. Phys.* **2002**, *117*, 7198.
(4) Nagai, H.; Carter, R. T.; Huber, J. R. *Chem. Phys. Lett.* **2000**, *331*, 425.
(5) Brock, L. R.; Rohlfing, E. A. *J. Chem. Phys.* **1997**, *106*, 10048.
(6) Osborn, D. L.; Choi, H.; Mordaunt, D. H.; Bise, R. T.; Neumark, D. M.; McMichael Rohlfing, C. *J. Chem. Phys.* **1997**, *106*, 3049.
(7) Alconcel, L. S.; Deyerl, H. J.; Zengin, V.; Continetti, R. E. *J. Phys. Chem. A* **1999**, *103*, 9190.
(8) Alconcel, L. S.; Deyerl, H. J.; Continetti, R. E. *J. Am. Chem. Soc.* **2001**, *123*, 12675.
(9) Ervin, K. M.; Lineberger, W. C. In *Advances in Gas-Phase Ion Chemistry*; Adams, N. G., Babcock, L. M., Eds.; JAI Press: Greenwich, CT, 1992; Vol. 1, p 121.
(10) Pinare, J. C.; Baguenard, B.; Bordas, C.; Broyer, M. *Phys. Rev. Lett.* **1998**, *81*, 2225.
(11) Deyerl, H. J.; Alconcel, L. S.; Continetti, R. E. *J. Phys. Chem. A* **2001**, *105*, 552.
(12) Surber, E.; Mabbs, R.; Sanov, A. *J. Phys. Chem. A* **2003**, *107*, 8215.
(13) Davis, A. V.; Wester, R.; Bragg, A. E.; Neumark, D. M. *J. Chem. Phys.* **2003**, *118*, 999.
(14) Reed, K. J.; Zimmerman, A. H.; Andersen, H. C.; Brauman, J. I. *J. Chem. Phys.* **1976**, *64*, 1368.
(15) Hanold, K. A.; Continetti, R. E. *Chem. Phys.* **1998**, *239*, 493.
(16) Ellison, G. B.; Engelking, P. C.; Lineberger, W. C. *J. Phys. Chem. A* **1982**, *86*, 4873.
(17) Mead, R. D.; Lykke, K. R.; Lineberger, W. C.; Marks, J.; Brauman, J. I. *J. Chem. Phys.* **1984**, *81*, 4883.
(18) Hunziker, H. E.; Kneppe, H.; Wendt, H. R. *J. Photochem.* **1981**, *17*, 377.
(19) Dupuis, M.; Wendoloski, J. J.; Lester, W. A. *J. Chem. Phys.* **1982**, *76*, 488.
(20) Sherwood, C. R.; Hanold, K. A.; Garner, M. C.; Strong, K. M.; Continetti, R. E. *J. Chem. Phys.* **1996**, *105*, 10803.
(21) Continetti, R. E. *Int. Rev. Phys. Chem.* **1998**, *17*, 227.
(22) Alconcel, L. S.; Deyerl, H. J.; DeClue, M.; Continetti, R. E. *J. Am. Chem. Soc.* **2001**, *123*, 3125.
(23) Zengin, V.; Persson, B. J.; Strong, K. M.; Continetti, R. E. *J. Chem. Phys.* **1996**, *105*, 9740.
(24) Chantry, P. J. *J. Chem. Phys.* **1969**, *51*, 3369.
(25) Osborn, D. L.; Leahy, D. J.; Kim, E. H.; de Beer, E.; Neumark, D. M. *Chem. Phys. Lett.* **1998**, *292*, 651.
(26) Continetti, R. E.; Cyr, D. R.; Neumark, D. M. *Rev. Sci. Instrum.* **1992**, *63*, 1840.
(27) Xie, X.; Simon, J. D. *Opt. Commun.* **1989**, 303.
(28) Davies, J. A.; LeClaire, J. E.; Continetti, R. E.; Hayden, C. C. *J. Chem. Phys.* **1999**, *111*, 1.
(29) Gebhardt, C. R.; Rakitzis, T. P.; Samartzis, P. C.; Ladopoulos, V.; Kitsopoulos, T. N. *Rev. Sci. Instrum.* **2001**, *72*, 3848.
(30) Townsend, D.; Minitti, M. P.; Suits, A. G. *Rev. Sci. Instrum.* **2003**, *74*, 2530.
(31) Lin, J. J.; Zhou, J.; Shiu, W.; Liu, K. *Rev. Sci. Instrum.* **2003**, *74*, 2495.
(32) Cooper, J.; Zare, R. N. *J. Chem. Phys.* **1968**, *48*, 942.
(33) Bragg, A. E.; Wester, R.; Davis, A. V.; Kammrath, A.; Neumark, D. M. *Chem. Phys. Lett.* **2003**, *376*, 767.
(34) Park, H.; Zare, R. N. *J. Chem. Phys.* **1996**, *104*, 4568.
(35) Mullin, A. S.; Murray, K. K.; Schulz, C. P.; Szaflarski, D. M.; Lineberger, W. C. *Chem. Phys.* **1992**, *166*, 207.